JOURNAL OF NEUROTRAUMA 38:1620–1631 (June 15, 2021)

DOI: 10.1089/neu.2020.7373

Tractography-Pathology Correlations in Traumatic Brain Injury: A TRACK-TBI Study

Amber L. Nolan,[1,2] Cathrine Petersen,[3] Diego Iacono,[4–8] Christine L. Mac Donald,[9] Pratik Mukherjee,[10] Andre van der Kouwe,[11] Sonia Jain,[12] Allison Stevens,[11] Bram R. Diamond,[11,13] Ruopeng Wang,[11] Amy J. Markowitz,[14] Bruce Fischl,[11,15] Daniel P. Perl,[4,5] Geoffrey T. Manley,[14] C. Dirk Keene,[1] Ramon Diaz-Arrastia,[16] and Brian L. Edlow[11,13]; and the TRACK-TBI Investigators*

Abstract

Diffusion tractography magnetic resonance imaging (MRI) can infer changes in network connectivity in patients with traumatic brain injury (TBI), but the pathological substrates of disconnected tracts have not been well defined because of a lack of high-resolution imaging with histopathological validation. We developed an *ex vivo* MRI protocol to analyze tract terminations at 750-μm isotropic resolution, followed by histopathological evaluation of white matter pathology, and applied these methods to a 60-year-old man who died 26 days after TBI. Analysis of 74 cerebral hemispheric white matter regions revealed a heterogeneous distribution of tract disruptions. Associated histopathology identified variable white matter injury with patchy deposition of amyloid precursor protein (APP), loss of neurofilament-positive axonal processes, myelin dissolution, astrogliosis, microgliosis, and perivascular hemosiderin-laden macrophages. Multiple linear regression revealed that tract disruption strongly correlated with the density of APP-positive axonal swellings and neurofilament loss. *Ex vivo* diffusion MRI can detect tract disruptions in the human brain that reflect axonal injury.

Keywords: contusion; MRI; neuropathology; tractography; traumatic axonal injury; traumatic brain injury

Introduction

Diffusion magnetic resonance imaging (dMRI) is used to study the neuroanatomic basis of altered consciousness and cognitive dysfunction in patients with traumatic brain injury (TBI).[1,2] dMRI images can map the structural connectivity of neural networks through the use of diffusion tractography, which has begun to reveal associations between brain network disconnections and their cognitive correlates.[3–8] As the field of ''connectomics'' has developed, symptom mapping has transitioned from focal lesion localization to a network-based connectivity paradigm.[9,10] For patients with TBI, this network-based approach to studying neurological deficits is particularly relevant, because disruption of neural networks by traumatic axonal injury (TAI) is one of the hallmark phenomena experienced by civilians[9] and military personnel[11] with head injury.

Yet, despite the contributions that diffusion tractography and the connectomics paradigm have made to the field of TBI, fundamental questions remain about the neuropathological substrates of tract disconnections. It is well established that diffusion tractography is susceptible to false positives (i.e., anatomically implausible tracts) and false negatives (i.e., tracts that terminate prematurely where

[1]Department of Laboratory Medicine and Pathology, [9]Department of Neurological Surgery, University of Washington, Seattle, Washington, USA.
[2]Department of Pathology, [3]Neuroscience Graduate Program, [10]Department of Radiology and Biomedical Imaging, University of California San Francisco, San Francisco, California, USA.
[4]Department of Pathology, [6]Department of Neurology, F. Edward Hébert School of Medicine, [5]DoD/USU Brain Tissue Repository (BTR) & Neuropathology Core, Uniformed Services University (USU), Bethesda, Maryland, USA.
[7]The Henry M. Jackson Foundation for the Advancement of Military Medicine (HJF), Bethesda, Maryland, USA.
[8]Complex Neurodegenerative Disorders, Motor Neuron Disorders Unit, National Institute of Neurological Disorders and Stroke (NINDS), National Institutes of Health (NIH), Bethesda, Maryland, USA.
[11]Athinoula A. Martinos Center for Biomedical Imaging, Department of Radiology, [13]Center for Neurotechnology and Neurorecovery, Department of Neurology, Massachusetts General Hospital and Harvard Medical School, Boston, Massachusetts, USA.
[12]Biostatistics Research Center, Herbert Wertheim School of Public Health and Human Longevity Science, University of California San Diego, San Diego, California, USA.
[14]Department of Neurological Surgery, University of California San Francisco, San Francisco, California, USA.
[15]Division of Health Sciences and Technology, Computer Science and Artificial Intelligence Laboratory (CSAIL), Massachusetts Institute of Technology, Cambridge, Massachusetts, USA.
[16]Department of Neurology, University of Pennsylvania, Philadelphia, Pennsylvania, USA.
*TRACK-TBI Investigators are listed in the Acknowledgments section at the end of the article.

axons remain intact).[12–14] However, observations about the limitations of diffusion tractography derive primarily from *ex vivo* magnetic resonance imaging (MRI) studies of normal, uninjured human brain specimens[15] and non-human primate brain specimens,[16,17] rather than analyses of human TBI brain specimens. Moreover, in the few studies that examined correlations between tract disruption and histopathology, the histological evaluation has been limited in scope, often focused only on axonal injury with reliance on amyloid precursor protein (APP) deposition to detect TAI.[18,19] As a result, it is unknown which of the many histopathological markers of axonal injury, or associated blood–brain barrier disruption and neuroinflammatory response, are associated with tract disruption in patients with TBI.

Here, we studied a human brain *ex vivo* from a patient enrolled in the longitudinal, observational Transforming Research and Clinical Knowledge in Traumatic Brain Injury (TRACK-TBI) study (https://tracktbi.ucsf.edu/transforming-research-and-clinical-knowledge-tbi). The patient had been admitted to the intensive care unit (ICU) and died of his injuries 26 days post-TBI. We conducted ultra-high-resolution diffusion tractography and comprehensive histological analyses to determine the neuropathological correlates of tract disruption. We performed multiple linear regression to test the hypothesis that the burden of histopathological axonal injury predicts the presence of tract disruption.

Methods

Case presentation

A 60-year-old man with a past medical history of Graves' disease and remote traumatic splenectomy was admitted to the hospital after a TBI. He was found down, unresponsive, next to his bicycle. An initial Glasgow Coma Scale (GCS) score of 9 (Eyes = 2, Motor = 5, and Verbal = 2) was reported in the field. On admission to the emergency department, he was severely agitated and found to have a right occipital hematoma. He was sedated and intubated. Neurological examination after intubation was again notable for a GCS score of 9, with movement in response to pain in all extremities, as well as intact pupillary, corneal, cough, and gag reflexes. Head computed tomography (CT) demonstrated a right parietal skull fracture, multi-focal bifrontal and temporal contusions with the largest in the left frontal lobe, a 6-mm left-sided subdural hemorrhage, diffuse convexal subarachnoid hemorrhage, and 5-mm left-to-right midline shift with transtentorial herniation.

Laboratory evaluation was notable for normal complete blood cell count, electrolyte panel, and renal and coagulation parameters. The patient was immediately taken to the operating room and treated with a decompressive left hemicraniectomy and external ventricular drain placement. A repeat head CT was notable for evacuation of the subdural hemorrhage and resolution of the midline shift, as well as blossoming of the contusions, mild worsening of transtentorial herniation, and uncal herniation. He was not on antiplatelet or anticoagulation medications before admission.

Within the first 3 days of admission to the ICU, the patient regained the ability to intermittently follow commands, and he was extubated on day 3 post-injury. However, his ICU course was complicated by a persistent fever of unknown etiology, aspiration events requiring re-intubation, focal seizure activity on electroencephalogram, a gastrointestinal bleed requiring transfusion, and progressive neurological worsening, such that he became unresponsive and developed extensor posturing in the upper extremities.

A 3 Tesla (T) brain MRI performed on day 13 post-injury demonstrated multi-focal hemorrhagic contusions in the bilateral frontal and temporal lobes, as well as right frontal subdural hemorrhage and hemorrhagic diffuse axonal injury in the midbrain (Supplementary Fig. S1). After several weeks without neurological improvement, the family transitioned the patient to comfort care, and he died on day 26 post-injury.

Before death, the patient was enrolled in the TRACK-TBI study. Written informed consent for brain donation was provided by the patient's surrogate decision maker. Inclusion criteria for TRACK-TBI have been previously reported and include age 0–100 and presentation at 1 of 18 enrolling Level 1 U.S. trauma centers within 24 h of injury, with external force trauma injury to the head warranting clinical evaluation with a non-contrast head CT evaluation based on current practice guidelines.[20] Exclusion criteria include pregnancy, ongoing life-threatening disease (such as end-stage malignancy), police custody, serious psychiatric and neurological disorders that would interfere with consent or follow-up outcome assessment, and non-English or Spanish (some sites) speakers. The study was approved by the institutional review board of each enrolling site.

In vivo *magnetic resonance imaging data acquisition and analysis*

In the *in vivo* component of this study, we focused on the susceptibility-weighted imaging (SWI) data set, which provides the highest sensitivity for detection of microhemorrhages and hemorrhagic contusions.[21] We (B.L.E., P.M.) analyzed the SWI data set for pathoanatomical lesions and classified each lesion using the National Institutes of Health (NIH), National Institute of Neurological Disorders and Stroke (NINDS) Common Data Elements (CDE) guidelines for TBI Neuroimaging.[22] We later applied this same lesion classification system to the *ex vivo* MRI 7T multi-echo fast low-angle shot (FLASH) sequence (MEF) data set to facilitate comparison of the *in vivo* and *ex vivo* lesion data.

Brain specimen acquisition and fixation

The whole brain was collected with a post-mortem interval of <24 h (Supplementary Fig. S2) and suspended in 10% formalin to facilitate adequate fixation, as previously described.[19] Before scanning, the brain specimen was transferred from 10% formalin to a Fomblin solution (perfluropolyether; Ausimont USA Inc., Thorofare, NJ) to reduce magnetic susceptibility artifacts and remove background signal.[23] The specimen, immersed in Fomblin, was packed in a vacuum-sealed bag to minimize air bubbles that would cause distortions in MRI data at the brain-air interface. Additional details regarding brain-specimen packing in preparation for *ex vivo* MRI scanning have been previously described.[19] After *ex vivo* imaging, the brain was placed back into 10% formalin until brain cutting was performed.

Ex vivo *magnetic resonance imaging acquisition*

We scanned the patient's brain using a 7T MRI scanner and 3T MRI scanner, as previously described.[19] Briefly, the 7T Siemens Magnetom MRI scan utilized a custom-built 31-channel receive array coil[24] and an MEF sequence[25] at 200-μm spatial resolution with the following echo times: 5.57/11.77/17.97/24.17 msec (Siemens, Erlangen, Germany). Total scan time on the 7T MRI scanner was 18 h and 31 min. The 3T Siemens Tim Trio MRI scan utilized a 32-channel head coil and a three-dimensional diffusion-weighted steady-state free-precession (DW-SSFP) sequence[26] at 750-μm spatial resolution. The DW-SSFP sequence included 90 diffusion-weighted volumes and 12 non-diffusion-weighted volumes (b = 0 s/mm^2). Of note, in a DW-SSFP sequence, diffusion weighting is not defined by a single global b value, because the diffusion signal cannot be readily dissociated from other imaging properties, such as the T_1 relaxation time, T_2 relaxation time, repetition time, and flip angle.[27] Total diffusion scan time on the 3T MRI scanner was

30 h and 31 min. All sequence parameters for the *ex vivo* 7T MEF and 3T DW-SSFP sequences have been previously reported.[19]

Ex vivo *magnetic resonance imaging processing and analysis*

The 7T MEF data were processed to create tissue parameter maps,[24] which were estimated directly from MEF acquisitions using the driven equilibrium single-pulse observation of T_1 (DESPOT1) algorithm.[25,28] Each parameter map provides quantification of tissue properties independent of scanner and sequence types. Parameter maps were combined to generate a synthetic FLASH scan with a flip angle of 20 degrees, determined to have the best overall contrast and better signal-to-noise ratio than each of the contributing scans (Supplementary Fig. S3).

The 3T DW-SSFP data were processed using the Diffusion Toolkit (version 6.4.1; http://trackvis.org/dtk) to reconstruct fiber tracts (i.e., streamlines), as previously described.[29] Notable processing parameters in the Diffusion Toolkit included: imaging model = HARDI/Q-Ball; angle threshold = 60 degrees; and propagation algorithm = FACT.

Magnetic resonance imaging–guided brain cutting, tissue sampling, and immunohistopathology

After imaging, the brainstem and cerebellum were removed, and the cerebral hemispheres were cut manually with a 300-mm blade by experienced neuropathologists (D.P.P., D.I.) into ~1-cm-thick serial coronal slabs and photographed (Supplementary Fig. S4), similar to a standard hospital autopsy procedure. Lesions and tissues of interest were then determined by a consensus video teleconference between investigators (A.L.N., R.D.-A., G.M., P.M., C.L.M., B.L.E., D.P.P., and D.I.) comparing gross morphology and anatomical landmarks on the coronal slabs with corresponding landmarks in the *ex vivo* and *in vivo* MRI. To study white matter in proximity to, and remote from, focal lesions, we (D.P.P., D.I.) performed tissue sampling for standard paraffin-embedded block preparation of brain parenchyma adjacent to the left inferior frontal lobe contusion, as well as in the contralateral inferior frontal lobe on the right, remote from any gross contusion or pathoanatomical lesions on imaging.

All tissue blocks were uniformly processed using an automated tissue processor (ASP 6025; Leica Biosystems, Nussloch, Germany). Standard hematoxylin and eosin stains, as well as immunohistochemical and special stains, were performed on serial 5-μm-thick sections. Special stains included Luxol fast blue (LFB). Immunohistochemical stains included antibodies against APP, glial fibrillary acidic protein (GFAP), ionized calcium-binding adapter molecule 1 (IBA1), and neurofilament, specifically to heavy-chain neurofilament (NF-H), which shows expression in uninjured axons.[30] All immunostains were performed using a Leica Bond III automated immunostainer with a diaminobenzidine chromogen detection system (DS9800; Leica Biosystems, Buffalo Grove, IL).

Specifications for each antibody are as follows: anti-APP (mouse antihuman monoclonal antibody clone 22c11, dilution 1:10, epitope retrieval time 10 min, MAB348; EMD Millipore, Burlington, MA); anti-GFAP (mouse antihuman monoclonal antibody GA5, with bond heat-induced epitope retrieval, epitope retrieval time 10 min, PA0026; Leica Biosystems, Wetzlar, Germany); anti-IBA1 (rabbit polyclonal, dilution 1:100, epitope retrieval time 10 min, Wako 016-20001; FUJIFILM Wako Pure Chemical Corporation, Osaka, Japan); and anti-NF-H (mouse antihuman monoclonal antibody SMI-34, dilution 1:100, epitope retrieval time 10 min, BioLegend 835503; BioLegend, San Diego, CA). Hemosiderin deposition was evaluated on a section with only counterstain. All stained slides were scanned at 20× magnification into digital images using the Aperio scanner system (Aperio AT2 - High Volume, Digital Whole Slide Scanning scanner; Leica Biosystems Inc., Richmond, IL) for analysis.

Region of interest selection for historadiological correlation analysis

To optimize the spatial alignment of the radiological and histopathological data, we rotated the coronal plane of the dMRI data set using FreeView software (https://surfer.nmr.mgh.harvard.edu/fswiki/FreeviewGuide) to align it with the coronal slab from the histopathological data set at the level of the inferior left frontal lobe contusion (Fig. 1 and Supplementary Fig. S5). After identifying anatomical coregistration landmarks in the contusional tissue, we determined that the optimal landmarks within the selected coronal slab for coregistration of non-contusional tissue were located in the contralateral frontal lobe, as shown in Supplementary Figure S6. Visual delineation of contusional and non-contusional anatomical landmarks was performed by a neuropathologist (A.L.N.), critical care neurologist (B.L.E.), and research technician (B.R.D.). Once an optimal rotation was agreed upon, this rotation of the dMRI data set was applied to the tractography data in TrackVis, allowing all tractography analyses to be performed in a spatial coordinate system that closely matched that of the chosen coronal gross pathology slabs.

Next, we created ''virtual slides'' in TrackVis with the same dimensions as the sampled tissue sections (Fig. 1 and Supplementary Figs. S5 and S6). Within each pair of virtual slides and histopathology slides, we created regions of interest (ROIs) for correlative tractography-histopathology analysis. These ROIs were matched through visual inspection, based upon the curvature of the gray-white junction and contusion profile. We placed the ROIs within the white matter, consistent with this study's aim of detecting the histopathological signatures of tract disruptions. Although directional water diffusion may be present within the gray matter of the cerebral cortex,[31] tracts typically terminate when they reach normal gray matter, and thus gray matter was not probed in this study.

We considered the optimal ROI size and shape for testing correlations between tract disruptions and histopathological markers of axonal white matter injury. We used a data-driven approach in which we analyzed clusters of disrupted tracts in white matter pathways that were not included in the virtual slides: the genu, body, and splenium of the corpus callosum (Supplementary Figs. S7 and S8). Visual analysis of disrupted tracts within these white matter bundles demonstrated that tract disruptions were typically localized to square-shaped clusters of four voxels in a 2×2 grid (1.5×1.5 mm) or smaller (Supplementary Figs. S7 and S8). Quantitative analysis of disrupted tracts within the splenium of the corpus callosum demonstrated that the most common motif for spatial arrangements of voxels with tract disruptions was a square-shaped 2×2 voxel arrangement. Voxels within this 2×2 motif totaled 32.9% (144 of 438) of all voxels with tract disruptions. The remaining disrupted tracts were in single voxels (4.8% of all disrupted tracts) or various irregularly shaped clusters (Supplementary Fig. S9).

Given this spatial distribution of tract disruptions, along with our goal of optimizing visual coregistration, we selected a square-shaped, 2×2 voxel ROI for testing tractography-pathology correlations in the virtual slides. Selection of smaller ROIs would have compromised the accuracy of the coregistration, whereas selection of larger ROIs would have lowered our statistical power to detect an association between tract disruption and histopathological signs of axonal injury, because intact tracts would have been interspersed with disconnected tracts within each ROI. Of note, we arranged groups of four ROIs in a square (8×8 voxels) to further optimize visual coregistration between the histopathology and tractography data and minimize the number of anatomical landmarks required to identify each ROI (Fig. 1 and Supplementary Figs. S5 and S6). Optimal sample size for our analysis was determined after performing a multiple regression power calculation using the pwr package in R (R Foundation for Statistical Computing, Vienna, Austria), based on a conservative estimate of $R^2 = 0.2$ from a preliminary analysis that included 15 ROIs. The alpha value was set to 0.05 and the power level set to 0.80.

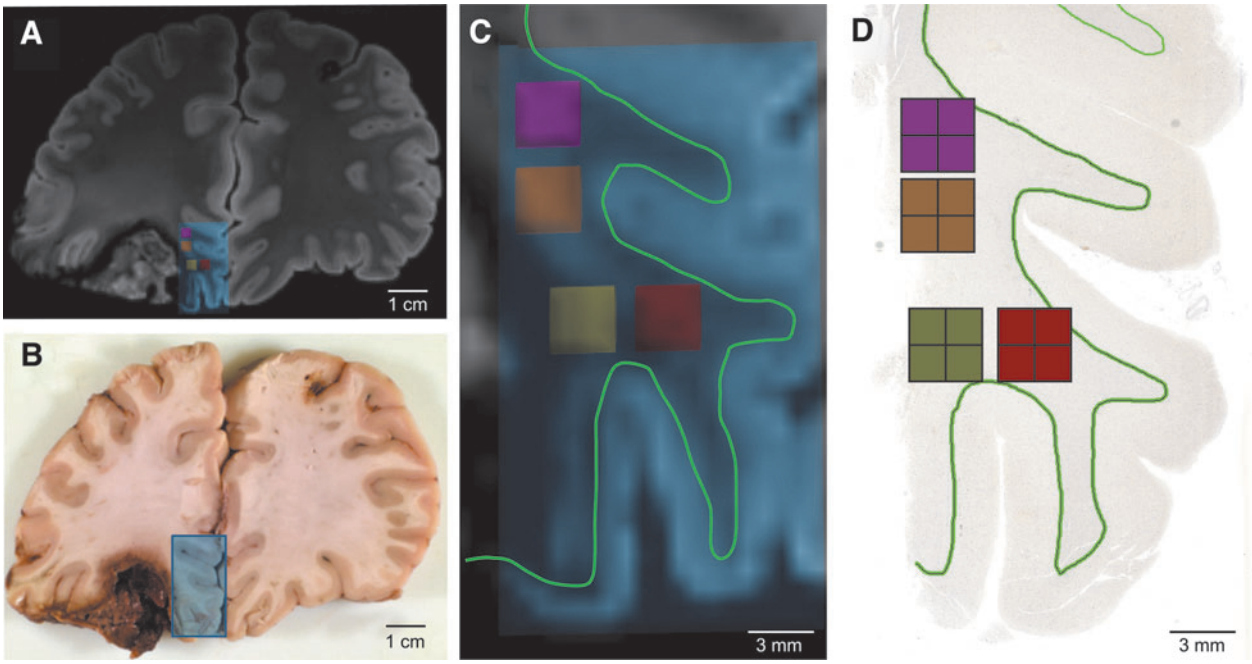

FIG. 1. Coregistration of pericontusional regions for analysis in *ex vivo* imaging and histologic sections. (**A**) Coronal section of MRI at the level of the left inferior frontal contusion. Blue box indicates area sampled for histology. (**B**) Gross pathology of the same region. Blue box indicates the tissue block taken for histology. (**C**) Magnification of area taken for histologic sampling from (A). Small pink, orange, yellow and red boxes indicate regions of analysis for tractography, which were co-registered to the histology by mapping their spatial relationship to the gray-white junction (green line). (**D**) Image of tissue section with pink, orange, yellow and red boxes indicating regions of analysis for histology. A green outline of the gray-white junction is shown in (D) to match the green outline shown in (C). MRI, magnetic resonance imaging.

Given this calculation, we then assessed 64 ROIs, of which most were placed >2 mm from the left inferior frontal contusion. However, we observed higher levels of tract disruption and prominent pathology in a few ROIs directly adjacent to the contusion. Given that this pathology is of biological significance, we believed that it should be well represented in our model, and thus we added 12 ROIs directly adjacent to the contusion (brown, cream, and light pink boxes in Supplementary Fig. S5). ROIs were excluded if no tracts were detected. Seventy-six ROIs were evaluated in total, and two were excluded.

Tractography analysis

Once ROI size and placement were determined within the virtual slides, we processed the *ex vivo* diffusion data set for deterministic tract construction using the Diffusion Toolkit, and we performed a tractography analysis: DISCONNECT (Delineation of Intact and Severed Components Of Neural NEtwork ConnecTions), using the TrackVis software (www.trackvis.org).[18] The DISCONNECT technique allows for a virtual dissection of disrupted fiber tracts from intact fiber tracts, with visualization and quantification of tract ''end-points'' that terminate within an ROI. Given that tracts are not expected to terminate within healthy white matter, the presence of a tract end-point is interpreted as inferential evidence of axonal injury, leading to a loss of directional water diffusion along the injured axon bundle. For this study, TrackVis creator Ruopeng Wang, MS, created new functionality in TrackVis that allows focused visualization of tract end-points within an ROI (i.e., without concurrently visualizing the other end of the tract). We release this new DISCONNECT functionality in an updated version of the TrackVis software program as version 0.6.3 (www.trackvis.org).

Histopathology analysis

To quantify white matter pathology and allow correlation with tractography, several metrics were extracted from scanned images of the immunohistochemical and special stains. Staining was quantified for APP, NF-H, GFAP, IBA1, and hemosiderin as follows: Aperio ImageScope© (Aperio ImageScope, version 2016; Leica Biosystems) was used to extract a tiff image containing four ROIs (each ROI, $1.5 \times 1.5\,mm^2$). All images were then processed and quantified using FIJI/ImageJ software (NIH, Bethesda, MD).[32] Each image was divided into 4 (for final ROIs) and converted into grayscale and then a binary image, using the same pre-determined threshold for every image. Expression or deposition was quantified as the percentage of area staining for NF-H, GFAP, IBA1, and hemosiderin.

To quantify APP, we identified swollen axons rather than an increase in expression, given that swollen axons may appear in a background of non-specific staining unrelated to accumulation from impaired transport. To this end, APP swellings were detected in ImageJ using the ''analyze particles'' function on the binary processed images with a size criterion of $>12.6\,\mu m^2$ and a circularity between 0.2 and 1. These values correspond to the size of axonal swellings that have been reported in TBI and fall within the range of criteria previously published.[33,34] Additionally, these values matched the swellings identified with visual inspection. The LFB-stained slide was quantified as the average intensity of staining on a red-green-blue image rather than the percent area after thresholding. In some ROIs, directly adjacent to the contusion edge, a small area without tissue was included within the $1.5 \times 1.5\,mm$ area. These ''blank'' areas were manually cropped from the image before analysis, and percentage of area or intensity of staining were only calculated within the tissue present.

Statistical analysis

Statistical analyses were performed using R Statistical Software (version 3.6.1; R Foundation for Statistical Computing). Univariate monotonic correlation between variables was analyzed using Spearman's correlation coefficient. Multiple linear regression evaluated the relationship between the percentage of disconnected

tracts and the standardized quantitative pathological data, including the number of APP^+ swellings/μm^2, percentage of staining for GFAP, IBA1, NF-H, and hemosiderin, and intensity of LFB. Predictor variables were mean-centered and scaled by 1 standard deviation (SD). These quantitative pathological variables were selected as the best indicators of the relative presence of each marker within each ROI. The percentage of disconnected tracts, rather than the number of disconnected tracts, was chosen as the outcome variable given the variability in tract number detected within the ROIs. Multi-collinearity among the predictors was investigated by using Spearman's correlation and the variance inflation factor. Sensitivity analysis was performed on the multiple linear regression model using the leave-one-out cross validation (LOOCV) method, whereby one observation was systematically removed from the model to evaluate the effect on the significance of the contributing variables. p values were calculated from two-sided tests in all cases, and p values <0.05 were considered statistically significant.

Results

In vivo *3 Tesla magnetic resonance imaging: lesion identification*

Classification of the *in vivo* SWI data set revealed multiple pathoanatomical lesions, which were classified using the NIH-NINDS CDE for TBI Neuroimaging (Supplementary Fig. S1; Supplementary Table S1). These lesions included a left frontal contusion, left temporal contusion, right frontal opercular contusion, right temporal contusion, intraventricular hemorrhage, and grade 3 diffuse axonal injury, as evidenced by traumatic microbleeds in the midbrain.

Ex vivo *7 Tesla magnetic resonance imaging: lesion identification*

A quality assessment (performed by B.L.E., B.F., A.v.d.K., A.S., and B.R.D.) of the 7T MRI data revealed excellent delineation of anatomical landmarks and minimal distortions related to air bubbles (Supplementary Fig. S3). Classification of the *ex vivo* MEF data set revealed multiple lesions that were similar in signal characteristic and neuroanatomical distribution to the lesions observed on *in vivo* 3T MRI (Supplementary Table S2; Supplementary Fig. S3).

Ex vivo *3 Tesla magnetic resonance imaging: tractography disconnection analysis*

Analysis of tract termination within each of 74 cerebral hemispheric white matter ROIs using the DISCONNECT tractography technique with TrackVis software (see Methods) revealed a wide range of tract disruption. Percentage of disrupted tracts ranged from 0% to 100%, with a mean $\pm$ SD tract disruption of $26.8 \pm 25.0\%$. These disconnections were particularly prominent in the pericontusional region, affecting multiple white matter bundles: the forceps minor (Fig. 2 and Supplementary Fig. S10), the cingulum bundle, the arcuate fasciculus, the medial forebrain bundle, and frontal cortico-cortical white matter bundles.

Overview of neuropathological findings

Macroscopic examination at autopsy revealed an edematous brain (formalin-fixed weight, 1785 g) with numerous contusions. The largest contusion was identified in the inferior left frontal lobe extending into the rostral left temporal lobe. The left frontal gyrus rectus remained intact, but the remainder of the left orbitofrontal and inferolateral temporal cortical surface was replaced by blood clot and granular tan-red tissue without identifiable gyral landmarks (Fig. 1 and Supplementary Figs. S2 and S4). A second contusion was noted in the right posterior frontal lobe localized to the inferior portion of the pre-central gyrus and abutting the lateral sulcus.

After sectioning of the brain, focal hemorrhage ($\sim$2–3 mm) was found in the midbrain adjacent to the left red nucleus. Finally, an external ventricular drain tract was identified in the right superior frontal gyrus extending through the right centrum semiovale and right genu of the corpus callosum. Patchy accumulation of blood products was also present over the dorsal aspects of the right cerebral hemisphere, consistent with organizing subdural and subarachnoid hemorrhage. Vessels of the circle of Willis and vertebrobasilar system were patent and intact and without significant atherosclerosis or other abnormality.

For the microscopic analysis, we focused on white matter pathology adjacent to the left inferior frontal contusion (Fig. 1 and Supplementary Fig. S5) and the grossly unremarkable white matter in the contralateral right medial and inferior frontal lobe (Supplementary Fig. S6). A series of special and immunohistochemical stains were performed on serial sections to evaluate axonal damage (APP accumulation and loss of phosphorylated NF-H), myelin integrity (LFB), reactive gliosis (GFAP, IBA1), and hemosiderin deposition (assessed on slide with only counterstain).

Adjacent to the left frontal contusion in a region with numerous disconnected tracts (Fig. 3), axonal pathology was prominent with frequent dot-like to globular deposition of APP. In addition, there was a loss of the usual fine fibrillar NF-H staining of axons in white matter replaced by more patchy granular deposits and occasional thickened linear fragments. An LFB stain was variable, but overall pale in intensity, consistent with severe myelin loss. Frequent GFAP-positive hypertrophic astrocytes were scattered throughout the white matter, and numerous reactive microglia with thickened processes and ameboid macrophages were identified with IBA1 staining. Hemosiderin-laden macrophages were often found adjacent to small capillaries.

In contrast, the grossly unremarkable white matter in the right hemisphere in a region with few disconnected tracts (Fig. 4) did not demonstrate significant APP deposition, exhibited a dense meshwork of fine NF-H-positive axonal processes, and displayed a more homogeneous and strong blue intensity with LFB staining. Scattered astrocytes with fine GFAP-positive processes were present, and IBA1 staining highlighted highly ramified microglia. Finally, significant hemosiderin deposition was not identified, supporting the impression of largely unremarkable white matter on histopathology and tractography. We release images of microscopic sections to the academic community at https://histopath.nmr.mgh.harvard.edu (TRACK-TBI Collection, Case ID ''TRACK-NP_001'').

Quantitative tractography-pathology correlation

To examine the relationship between individual histopathology metrics and the percentage of disrupted tracts, we first assessed monotonic association using Spearman's correlation coefficient. A positive correlation was identified between the density of APP^+ swellings (APP swellings/μm^2) and the percentage of disrupted tracts (Fig. 5; $r = 0.25$, confidence interval [CI] = [0.01, 0.45], $df = 72$, $p = 0.0345$); likewise, a negative correlation was found between NF-H staining (% area) and the percentage of disrupted tracts (Fig. 5; $r = -0.39$, CI = [–0.57, –0.17], $df = 72$, $p = 0.0006$). We then built a multiple linear regression model to evaluate how the percentage of disconnected tracts was related to the pathological variables in combination. Independent variables included the density of APP^+ swellings and the percentage area of staining

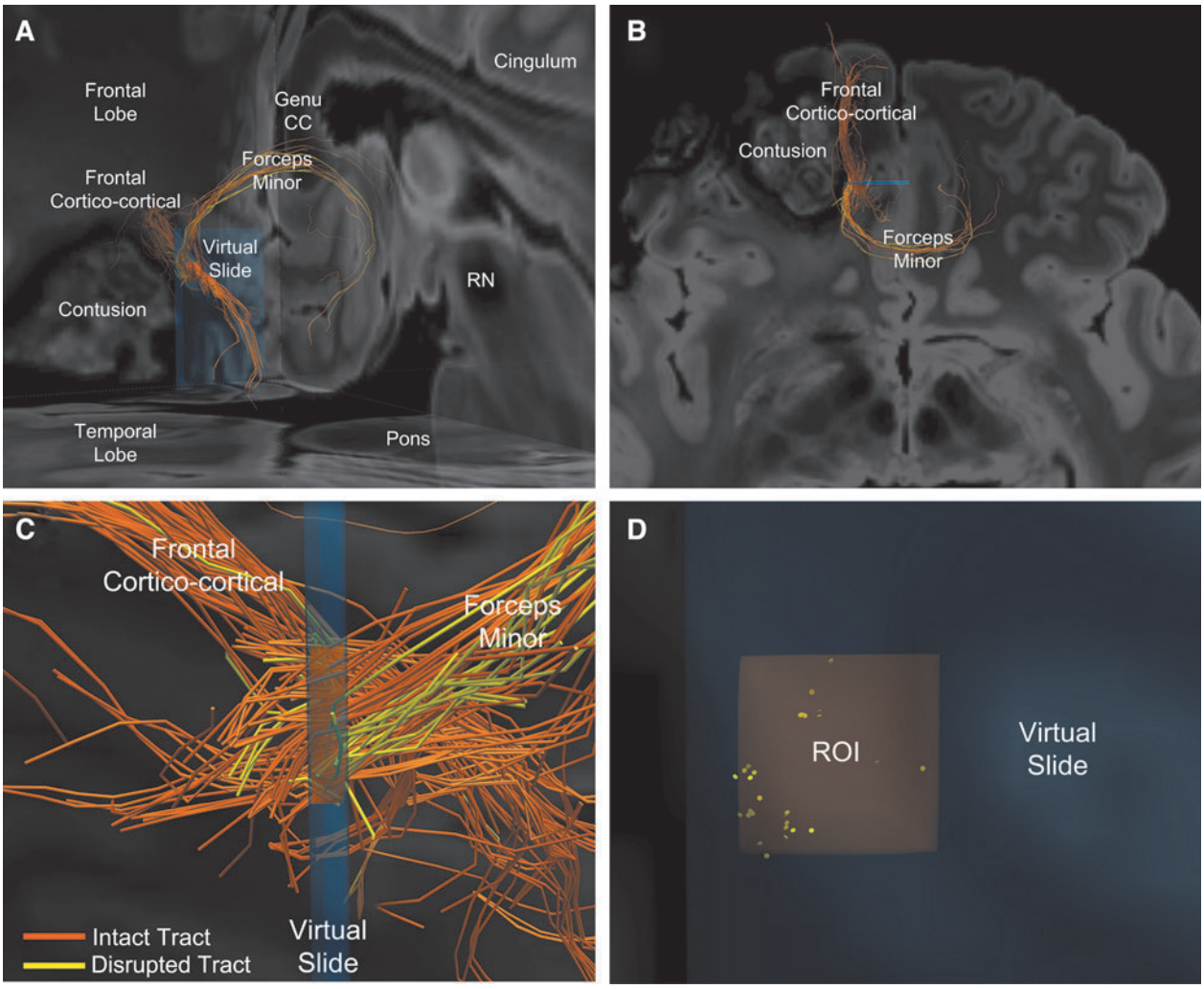

FIG. 2. Representative image of intact and disrupted tracts passing through a pericontusional region of interest (ROI). (**A**) Posterolateral oblique perspective of tracts passing through the orange ROI from Figure 1. Two bundles of tracts are identified: the forceps minor crossing the genu of the corpus callosum and a frontal cortico-cortical white matter bundle. (**B**) Higher magnification of image in (A), shown from a superior perspective. Orange indicates intact tracts, whereas yellow indicates disconnected tracts that terminate in the orange ROI. (**C**) Left lateral perspective of the orange ROI within the blue virtual slide. Intact (orange) and disconnected (yellow) tracts are seen within forceps minor and the frontal cortico-cortical bundles, with the former showing a higher percentage of disrupted tracts. (**D**) Anterior view of disconnected tract endpoints (yellow discs) within the orange ROI reveals that the tracts tend to be disconnected in small clusters. CC, corpus callosum; RN, red nucleus.

within the ROIs for GFAP, IBA1, NF-H, and hemosiderin, as well as the intensity of LFB staining. For standardization, the independent variables were mean-centered and scaled by 1 SD. The dependent variable was the percentage of disconnected tracts within the ROIs. In the multiple linear regression model, the density of APP^+ swellings and the percentage area of staining for NF-H and hemosiderin were the only variables to have a significant effect on the percentage of disconnected tracts ($\beta = 9.5$, CI = [4.1, 15.0], $p = 0.0009$; $\beta = -11.8$, CI = [−17.4, −6.2], $p = 0.0001$; and $\beta = 6.1$, CI = [1.0, 11.3], $p = 0.0209$; respectively, $df = 67$; Table 1).

To ensure the robustness of these results, a sensitivity analysis was performed using the LOOCV method. The density of APP^+ swellings and the percentage area of NF-H staining were significantly correlated in all models with the percentage of disconnected tracts (all $p < 0.05$). However, two influential ROIs were identified as driving the hemosiderin correlation, and when removed, a significant relationship was no longer observed between the percentage area of hemosiderin staining and the percentage of disconnected tracts ($\beta = 4.8$, CI = [–0.9, 10.5], $p = 0.0999$, Supplementary Table S3; $\beta = 4.2$, CI = [−1.0, 9.5], $p = 0.1031$, Supplementary Table S4).

Discussion

In this correlative historadiological analysis of a patient who died in the ICU from TBI, we provide evidence for a link between tract disruption and axonal injury in the human brain. Whereas previous historadiological analyses of humans with TBI exposure provided qualitative evidence that tract disruption occurs in anatomic proximity to axonal injury,[18] we implemented a quantitative approach in which ROI-based measures of tract injury were tested for correlations with gold-standard measures of white matter injury, including markers of axonal injury, demyelination, neuroinflammation, and vascular pathology. We observed that disruption of fiber tracts on *ex vivo* diffusion tractography MRI was strongly

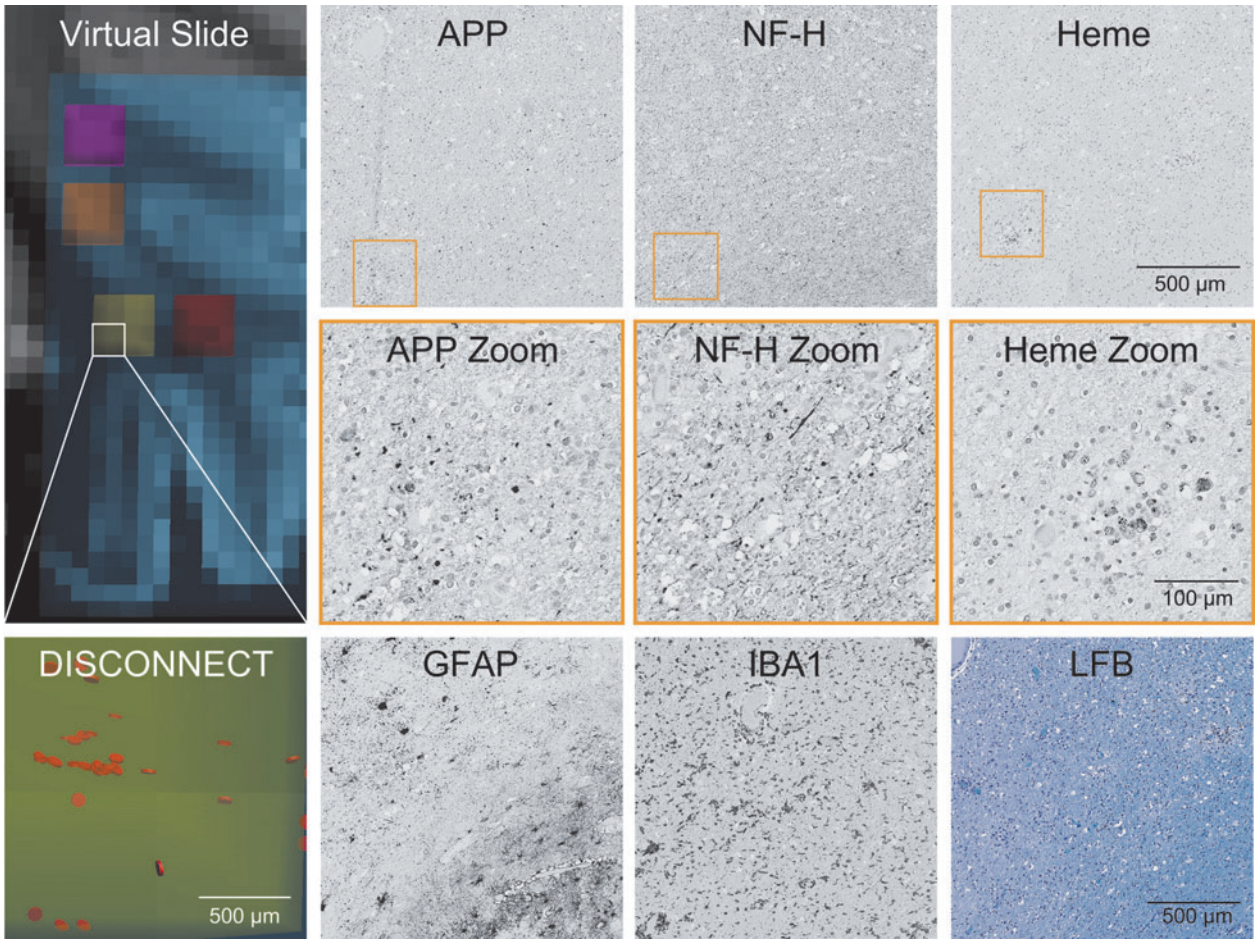

FIG. 3. Representative histology of pericontusional region of interest with numerous disrupted tracts. The virtual slide demonstrates a pericontusional region on MRI and the associated disrupted tracts by DISCONNECT analysis; disrupted tracts are shown in orange. In the same region of interest, images are shown for immunohistochemistry of amyloid precursor protein (APP), neurofilament (NF-H), glial fibrillary acidic protein (GFAP), and ionized calcium-binding adaptor molecule 1 (IBA1). Hemosiderin (Heme) deposition is identified on a counterstained slide. A Luxol fast blue (LFB) stain indicative of myelin is also displayed. Substantial deposition of APP and a lack of fine background processes with only course sparse swollen segments with NF-H is seen, consistent with the large number of disrupted tracts identified in this region. MRI, magnetic resonance imaging.

associated with the density of APP^+ swellings and loss of neurofilament staining. These findings indicate that tract disruptions reflect axonal injury in human patients with TBI.

Our findings are consistent with, and build upon, previous animal studies and limited human studies that assessed correlations between dMRI metrics and histopathological axonal injury. Corresponding to our findings, Mac Donald and colleagues identified that anisotropy correlated with the density of APP-positive axons in a mouse model of moderate-to-severe focal contusion injury.[35] Similarly, a model of Wallerian degeneration after dorsal root axotomy in the rat revealed reduced parallel diffusivity *in vivo* within the ipsilateral dorsal column, correlating with loss of a phosphorylated NF-H, over a span of 3–30 days after injury.[36] In an animal model of repetitive rotational head acceleration, patterns of white matter tract damage identified by reduced fractional anisotropy were comparable to white matter injury identified by increased silver staining[37]; likewise, silver staining reflected relative anisotropy in the corpus callosum in another mild repetitive closed TBI model.[38] In human tissue, a correlation was identified between fractional anisotropy and axonal disruption, as measured by the power coherence of myelin black gold staining at a resolution of $250\times 250\times 500\ \mu m^3$, in cases of chronic traumatic encephalopathy.[39]

Although tractography has been shown to predict cognitive and focal motor deficits in humans with severe TBI,[3,40] few studies have directly examined correlations between tract disconnections and histological axonal metrics. One study of a patient with traumatic coma evaluated spatial patterns of tract disruption with pathology, finding a similar qualitative distribution of APP immunohistochemistry and disconnected tracts near a brainstem hemorrhage.[18] Here, we provide quantitative correlation of disconnected tracts—both nearby and remote from a focal hemorrhage—with numerous pathological indices, including measures of axonal damage and integrity, neuroinflammation, and vascular pathology.

Notably, the density of APP^+ swellings and neurofilament staining carried similar weights in the multiple linear regression model. This finding suggests that both metrics are important in quantifying axonal injury rather than only examining APP deposition, which is the standard method in many studies. Indeed, animal models suggest that APP alone is not sufficient to detect all types of axonal injury. For example, specific neurofilament epitopes and an N-terminal fragment of the α-spectrin protein accumulate in swollen axons that do not coexpress APP,[33,41] and transgenic labeling of axons in mice shows numerous axonal swellings and transections without APP accumulation after TBI.[42]

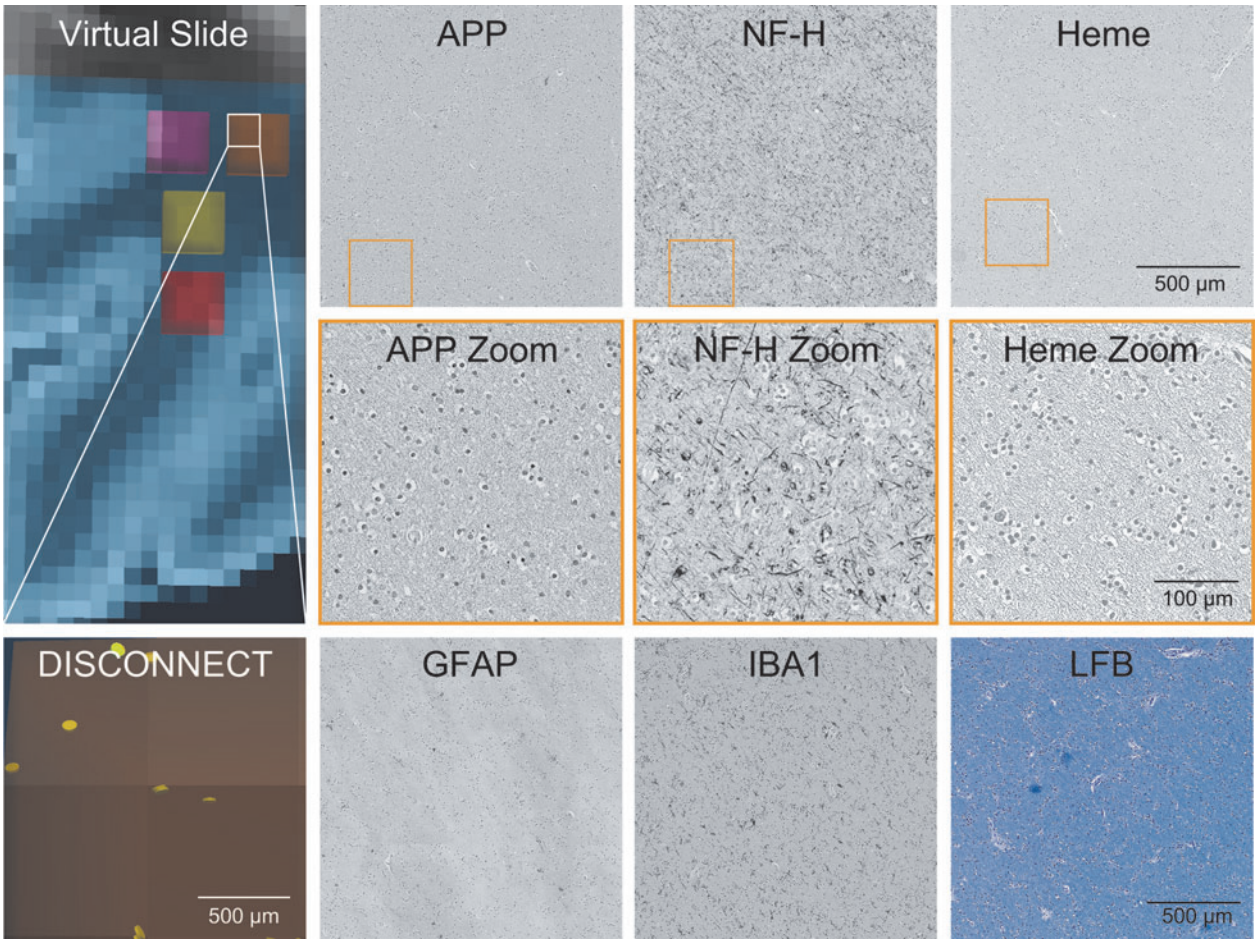

FIG. 4. Representative histology of contralateral region of interest with few disrupted tracts. The virtual slide demonstrates a contralateral region on MRI in an area grossly intact and the associated disrupted tracts by DISCONNECT analysis; disrupted tracts are shown in yellow. In the same region of interest, images are shown for immunohistochemistry of amyloid precursor protein (APP), neurofilament (NF-H), glial fibrillary acidic protein (GFAP), and ionized calcium binding adaptor molecule 1 (IBA1). Hemosiderin (Heme) deposition is identified on a counterstained slide. A Luxol fast blue (LFB) stain indicative of myelin is also displayed. Minimal APP deposition and numerous fine background axonal processes with NF-H are seen, consistent with the small number of disrupted tracts identified in this region. MRI, magnetic resonance imaging.

Further, APP accumulation does not always represent axonal transection and may not indicate impending disconnection.[43] Neurofilament loss, a direct indicator of axon loss, may thus be an important metric to identify axonal injury that is not apparent with APP staining alone, especially when correlating with tractography in a patient who died weeks after TBI. Future studies are needed to determine how disconnected tracts correlate with different markers of axonal injury and integrity at acute to chronic time points with variable injury mechanisms.

Intriguingly, indices of neuroinflammation measured with GFAP and IBA1 immunohistochemistry and myelin evaluated with LFB staining were not associated with disconnected tracts, but microvascular disruption quantified by hemosiderin deposition was a significant variable in our model when including all histological metrics and all ROIs. However, two influential, pericontusional ROIs were identified by sensitivity analysis. This observation suggests that vascular disruption can influence tractography in a specific context, such as in pericontusional locations. Vascular pathology has not been routinely included as a pathological metric in studies of dMRI radiological-pathological correlation. However, T_2*-weighted MRI post-mortem imaging has found that traumatic microbleeds defined by small foci of hypointensity represent the accumulation of perivascular iron-laden macrophages, and that this imaging metric is correlated with worse outcome in TBI.[44] Indeed, blood–brain barrier disruption and microvascular pathology have been found to be widespread even in less-severe TBI and partially overlap with regions of axonal injury.[45]

Post-mortem MRI has been proposed as an adjuvant to standard neuropathological assessment,[46] given that *ex vivo* MRI measures of white matter integrity may help to elucidate the neuroanatomic basis of altered consciousness and cognitive deficits observed antemortem.[18,19,47] DISCONNECT analysis and tractography with post-mortem dMRI may further highlight subtle axonal pathology not routinely examined with standard neuropathology. Use of these techniques will improve our understanding of the structural connectome of the brain even after death and fundamentally bridge how *in vivo* imaging metrics are related to complex microstructural alterations at the molecular level. Furthermore, high-resolution *ex vivo* MRI methods, when performed in conjunction with gold-standard histopathological validation, may elucidate how the magnetic susceptibility effects of blood affect the reliability of tractography data in regions of hemorrhagic axonal injury.

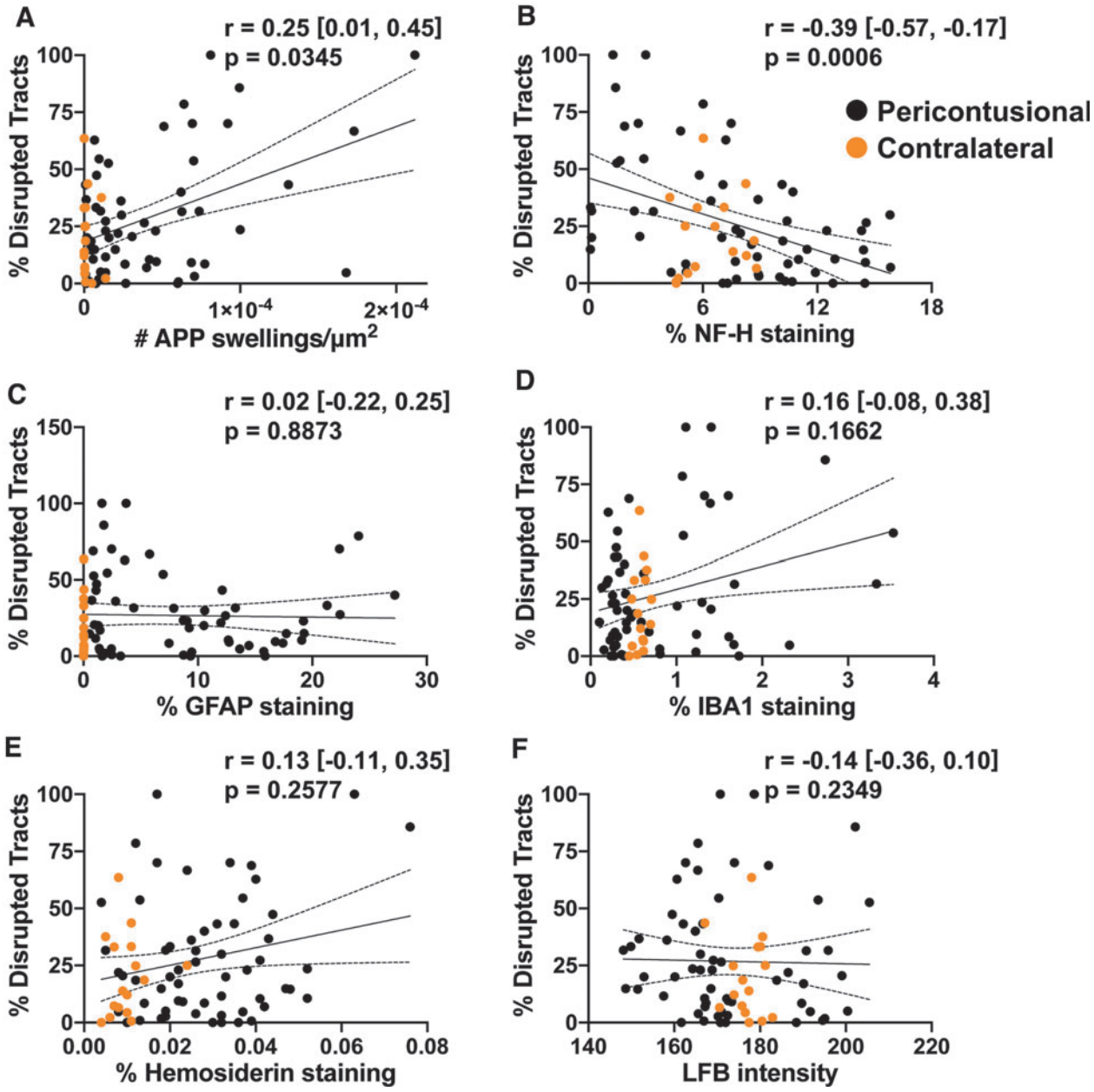

FIG. 5. Correlations of pathology with tractography. Univariate linear regressions for each marker against % tracts disrupted are plotted: (**A**) amyloid precursor protein (APP), (**B**) neurofilament (NF-H), (**C**) glial fibrillary acidic protein (GFAP), (**D**) ionized calcium-binding adaptor molecule 1 (IBA1), (**E**) hemosiderin, and (**F**) Luxol fast blue (LFB). The Spearman's correlation coefficient (r) with the confidence intervals and the associated *p* value is provided for each pair. Degrees of freedom for each test = 72. Individual data points are solid circles: black denotes pericontusional, and orange denotes contralateral regions of interest. The solid line indicates the best linear fit; dotted lines indicate the 95% confidence intervals.

Strengths of this study include direct quantitative correlation of numerous metrics of white matter pathology after TBI, not only axonal injury, but also gliosis, myelination, and vascular injury, with tract disconnections identified by ultra-high-resolution tractography—an evaluation that has not been performed before in human TBI. However, several limitations should be considered when interpreting our findings. In particular, these analyses were performed in a single patient who died several weeks after injury. The pathology identified here may be multi-factorial, involving pathophysiological processes such as edema and resulting local and global ischemia/hypoxia in addition to TAI. It remains to be determined whether these significant relationships are observed in TAI throughout the brain, not just pericontusional white matter, as well as other cases at variable acute, subacute, and chronic time points with variable mechanisms of TBI.

Furthermore, the coregistration of *ex vivo* MRI data and histopathological data was performed visually without advanced imaging techniques to correct for the known non-linear transformations that occur with tissue processing.[48] Although the sections and ROIs used for analysis were specifically chosen to best recapitulate the relationship to the pattern of undulation of the gray-white matter junction, we cannot have achieved perfect overlap between the ROIs on

Table 1. Multiple Linear Regression Analysis

Variables	*Percentage of disrupted tracts*
No. of APP swellings/μm^2	9.5 [4.1, 15.0]
p value	***0.0009***
NF-H % area	–11.8 [–17.4, –6.2]
p value	***0.0001***
GFAP % area	–1.9 [–7.4, 3.5]
p value	*0.4809*
IBA1 % area	0.7 [–6.4, 7.8]
p value	*0.8462*
Heme % area	6.1 [1.0, 11.3]
p value	***0.0209***
LFB intensity	–2.4 [–9.0, 4.2]
p value	*0.4643*

Degrees of freedom = 67.

Coefficient [95% confidence interval].

APP, amyloid precursor protein; NF-H, neurofilament; GFAP, glial fibrillary acidic protein; IBA1, ionized calcium-binding adaptor molecule 1; Heme, hemosiderin; LFB, luxol fast blue.

imaging and pathology. Future studies are needed to optimize co-egistration of *ex vivo* post-mortem MRI data with tissue sampling and analysis.

In summary, we show that axonal injury and, possibly, microvascular disruption may be important indices influencing diffusion tractography disconnections in TBI. Future work will address the reproducibility and nuances of these relationships in a wider patient population, providing a foundational understanding of network-based *ex vivo* imaging analyses that bridge the methodological gap between microscopy and *in vivo* MRI in human patients with TBI.

Data Availability

The data set used for final analysis is provided as a supplemental Excel file; raw data are shown in Figure 5. Histopathological images are available at https://histopath.nmr.mgh.harvard.edu (TRACK-TBI Collection, Case ID ''TRACK-NP_001''). The DISCONNECT functionality for tract termination visualization is available in an updated version of the TrackVis software program as version 0.6.3 (www.trackvis.org). Additional data requests can be made to the corresponding author.

Acknowledgments

We thank the patient and family for their participation in the TRACK-TBI study and for their generous donation of the post-mortem brain.

The opinions expressed here are those of the authors and are not necessarily representative of those of the Uniformed Services University, the United States Department of Defense, or the United States Army, Navy, or Air Force or any other federal agency.

The TRACK-TBI Investigators

Opeolu Adeoye, University of Cincinnati; Neeraj Badjatia, University of Maryland; Kim Boase, University of Washington; Jason Barber, University of Washington; Yelena Bodien, Massachusetts General Hospital; M. Ross Bullock, University of Miami; Randall Chesnut, University of Washington; John D. Corrigan, Ohio State University; Karen Crawford, University of Southern California; Ramon Diaz-Arrastia, University of Pennsylvania; Sureyya Dikmen, University of Washington; Ann-Christine Duhaime, MassGeneral Hospital for Children; Richard Ellenbogen, University of Washington; V. Ramana Feeser, Virginia Commonwealth University; Adam R. Ferguson, University of California, San Francisco; Brandon Foreman, University of Cincinnati; Raquel Gardner, University of California, San Francisco; Etienne Gaudette, University of Southern California; Joseph Giacino, Spaulding Rehabilitation Hospital; Dana Goldman, University of Southern California; Luis Gonzalez, TIRR Memorial Hermann; Shankar Gopinath, Baylor College of Medicine; Rao Gullapalli, University of Maryland; J. Claude Hemphill, University of California, San Francisco; Gillian Hotz, University of Miami; Sonia Jain, University of California, San Diego; C. Dirk Keene, University of Washington; Frederick K. Korley, University of Michigan; Joel Kramer, University of California, San Francisco; Natalie Kreitzer, University of Cincinnati; Harvey Levin, Baylor College of Medicine; Chris Lindsell, Vanderbilt University; Joan Machamer, University of Washington; Christopher Madden, UT Southwestern; Geoffrey T. Manley, University of California, San Francisco; Alastair Martin, University of California, San Francisco; Thomas McAllister, Indiana University; Michael McCrea, Medical College of Wisconsin; Randall Merchant, Virginia Commonwealth University; Pratik Mukherjee, University of California, San Francisco; Lindsay Nelson, Medical College of Wisconsin; Laura B. Ngwenya, University of Cincinnati; Florence Noel, Baylor College of Medicine; Amber Nolan, University of California, San Francisco; David Okonkwo, University of Pittsburgh; Eva Palacios, University of California, San Francisco; Daniel Perl, Uniformed Services University; Ava Puccio, University of Pittsburgh; Miri Rabinowitz, University of Pittsburgh; Claudia Robertson, Baylor College of Medicine; Jonathan Rosand, Massachusetts General Hospital; Angelle Sander, Baylor College of Medicine; Gabriella Satris, University of California, San Francisco; David Schnyer, UT Austin; Seth Seabury, University of Southern California; Mark Sherer, TIRR Memorial Hermann; Murray Stein, University of California, San Diego; Sabrina Taylor, University of California, San Francisco; Nancy Temkin, University of Washington; Arthur Toga, University of Southern California; Alex Valadka, Virginia Commonwealth University; Mary Vassar, University of California, San Francisco; Paul Vespa, University of California, Los Angeles; Kevin Wang, University of Florida; John K. Yue, University of California, San Francisco; Esther Yuh, University of California, San Francisco; Ross Zafonte, Harvard Medical School.

Authors' Contributions

A.L.N. and B.L.E. conceptualized the study. A.L.N. analyzed the histopathology data. B.L.E. analyzed the tractography data. C.P. performed the statistical analysis and modeling. S.J. provided critical input for the statistical analysis. A.L.N. and B.L.E. wrote the manuscript. D.I. and D.P.P. assisted with the neuropathology characterization, tissue sampling, immunohistochemical staining, and slide scanning. C.L.M. and P.M. assisted with radiological-pathological correlation for tissue sampling and provided methodological input. A.v.d.K., A.S., B.R.D., R.W., and B.F. assisted with *ex vivo* imaging acquisition, processing, tractography analysis, and methodological input. A.J.M. edited the manuscript. G.T.M., C.D.K., and R.D-A. provided methodological input and interpretation of results. All authors revised the manuscript and provided critical feedback.

Funding Information

The study was funded by the NIH National Institute of Neurological Disorders and Stroke (U01NS086090, K08NS114170,

R21NS109627, RF1NS115268, K23NS094538, R01NS0525851, R21NS072652, R01NS070963, R01NS083534, U01NS086625, U24NS10059103, and R01NS105820), NIH Director's Office (DP2HD101400), NIH National Institute for Biomedical Imaging and Bioengineering (P41EB015896, 1R01EB023281, R01EB006758, R21EB018907, and R01EB019956), NIH National Institute on Aging (R56AG064027, R01AG064027, R01AG008122, and R01AG016495), NIH National Institute of Diabetes and Digestive and Kidney Diseases (R21DK108277), the United States Department of Defense (W81XWH-14-2-0176, W81XWH-18-2-0042, and W81XWH-15-9-0001), the James S. McDonnell Foundation, Abbott Point of Care Inc (A133407; G.T.M.), the National Football League Scientific Advisory Board (131769A), the Tiny Blue Dot Foundation, and the Nancy and Buster Alvord endowment (C.D.K.). This research also utilized resources provided by NIH shared instrumentation grants S10RR023401, S10RR019307, and S10RR023043. Additional support was provided by the BRAIN Initiative Cell Census Network (U01MH117023) and the NIH Blueprint for Neuroscience Research (5U01-MH093765), part of the multi-institutional Human Connectome Project, and One Mind.

Author Disclosure Statement

Dr. Fischl has a financial interest in CorticoMetrics, a company whose medical pursuits focus on brain imaging and measurement technologies. His interests were reviewed and are managed by Massachusetts General Hospital and Partners HealthCare in accordance with their conflict of interest policies.

The United States Department of Energy supports Dr. Manley for a precision medicine collaboration. One Mind has provided funding for TRACK-TBI patient stipends and support to clinical sites. Dr. Manley has received an unrestricted gift from the NFL to the UCSF Foundation to support research efforts of the TRACK-TBI NETWORK. Dr. Manley has also received funding from NeuroTrauma Sciences LLC to support TRACK-TBI data curation efforts. Additionally, Abbott Laboratories has provided funding for add-in TRACK-TBI clinical studies.

Ms. Markowitz receives salary support from the United States Department of Energy precision medicine collaboration and One Mind.

References

1. Hulkower, M.B., Poliak, D.B., Rosenbaum, S.B., Zimmerman, M.E., and Lipton, M.L. (2013). A decade of DTI in traumatic brain injury: 10 years and 100 articles later. AJNR Am. J. Neuroradiol. 34, 2064–2074.
2. Edlow, B.L., and Wu, O. (2012). Advanced neuroimaging in traumatic brain injury. Semin. Neurol. 32, 372–398.
3. Wang, J.Y., Bakhadirov, K., Abdi, H., Devous, M.D., Sr., Marquez de la Plata, C.D., Moore, C., Madden, C.J., and Diaz-Arrastia, R. (2011). Longitudinal changes of structural connectivity in traumatic axonal injury. Neurology 77, 818–826.
4. Newcombe, V.F., Williams, G.B., Scoffings, D., Cross, J., Carpenter, T.A., Pickard, J.D., and Menon, D.K. (2010). Aetiological differences in neuroanatomy of the vegetative state: insights from diffusion tensor imaging and functional implications. J. Neurol. Neurosurg. Psychiatry 81, 552–561.
5. Fernandez-Espejo, D., Soddu, A., Cruse, D., Palacios, E.M., Junque, C., Vanhaudenhuyse, A., Rivas, E., Newcombe, V., Menon, D.K., Pickard, J.D., Laureys, S., and Owen, A.M. (2012). A role for the default mode network in the bases of disorders of consciousness. Ann. Neurol. 72, 335–343.
6. Snider, S.B., Bodien, Y.G., Bianciardi, M., Brown, E.N., Wu, O., and Edlow, B.L. (2019). Disruption of the ascending arousal network in acute traumatic disorders of consciousness. Neurology 93, e1281–e1287.
7. Brandstack, N., Kurki, T., and Tenovuo, O. (2013). Quantitative diffusion-tensor tractography of long association tracts in patients with traumatic brain injury without associated findings at routine MR imaging. Radiology 267, 231–239.
8. Wang, J.Y., Bakhadirov, K., Devous, M.D., Sr., Abdi, H., McColl, R., Moore, C., Marquez de la Plata, C.D., Ding, K., Whittemore, A., Babcock, E., Rickbeil, T., Dobervich, J., Kroll, D., Dao, B., Mohindra, N., Madden, C.J., and Diaz-Arrastia, R. (2008). Diffusion tensor tractography of traumatic diffuse axonal injury. Arch. Neurol. 65, 619–626.
9. Sharp, D.J., Scott, G., and Leech, R. (2014). Network dysfunction after traumatic brain injury. Nat. Rev. Neurol. 10, 156–166.
10. Fox, M.D. (2018). Mapping symptoms to brain networks with the human connectome. N. Engl. J. Med. 379, 2237–2245.
11. Mac Donald, C.L., Johnson, A.M., Cooper, D., Nelson, E.C., Werner, N.J., Shimony, J.S., Snyder, A.Z., Raichle, M.E., Witherow, J.R., Fang, R., Flaherty, S.F., and Brody, D.L. (2011). Detection of blast-related traumatic brain injury in U.S. military personnel. N. Engl. J. Med. 364, 2091–2100.
12. Jones, D.K., Knosche, T.R., and Turner, R. (2013). White matter integrity, fiber count, and other fallacies: the do's and don'ts of diffusion MRI. Neuroimage 73, 239–254.
13. Jbabdi, S., and Johansen-Berg, H. (2011). Tractography: where do we go from here? Brain Connect. 1, 169–183.
14. Mukherjee, P., Chung, S.W., Berman, J.I., Hess, C.P., and Henry, R.G. (2008). Diffusion tensor MR imaging and fiber tractography: technical considerations. AJNR Am. J. Neuroradiol. 29, 843–852.
15. Edlow, B.L., Takahashi, E., Wu, O., Benner, T., Dai, G., Bu, L., Grant, P.E., Greer, D.M., Greenberg, S.M., Kinney, H.C., and Folkerth, R.D. (2012). Neuroanatomic connectivity of the human ascending arousal system critical to consciousness and its disorders. J. Neuropathol. Exp. Neurol. 71, 531–546.
16. Thomas, C., Ye, F.Q., Irfanoglu, M.O., Modi, P., Saleem, K.S., Leopold, D.A., and Pierpaoli, C. (2014). Anatomical accuracy of brain connections derived from diffusion MRI tractography is inherently limited. Proc. Natl. Acad. Sci. U. S. A. 111, 16574–16579.
17. Schmahmann, J.D., Pandya, D.N., Wang, R., Dai, G., D'Arceuil, H.E., de Crespigny, A.J., and Wedeen, V.J. (2007). Association fibre pathways of the brain: parallel observations from diffusion spectrum imaging and autoradiography. Brain 130, 630–653.
18. Edlow, B.L., Haynes, R.L., Takahashi, E., Klein, J.P., Cummings, P., Benner, T., Greer, D.M., Greenberg, S.M., Wu, O., Kinney, H.C., and Folkerth, R.D. (2013). Disconnection of the ascending arousal system in traumatic coma. J. Neuropathol. Exp. Neurol. 72, 505–523.
19. Edlow, B.L., Keene, C.D., Perl, D.P., Iacono, D., Folkerth, R.D., Stewart, W., Mac Donald, C.L., Augustinack, J., Diaz-Arrastia, R., Estrada, C., Flannery, E., Gordon, W.A., Grabowski, T.J., Hansen, K., Hoffman, J., Kroenke, C., Larson, E.B., Lee, P., Mareyam, A., McNab, J.A., McPhee, J., Moreau, A.L., Renz, A., Richmire, K., Stevens, A., Tang, C.Y., Tirrell, L.S., Trittschuh, E.H., van der Kouwe, A., Varjabedian, A., Wald, L.L., Wu, O., Yendiki, A., Young, L., Zollei, L., Fischl, B., Crane, P.K., and Dams-O'Connor, K. (2018). Multimodal characterization of the late effects of traumatic brain injury: a methodological overview of the late effects of traumatic brain injury project. J. Neurotrauma 35, 1604–1619.
20. Yue, J.K., Yuh, E.L., Korley, F.K., Winkler, E.A., Sun, X., Puffer, R.C., Deng, H., Choy, W., Chandra, A., Taylor, S.R., Ferguson, A.R., Huie, J.R., Rabinowitz, M., Puccio, A.M., Mukherjee, P., Vassar, M.J., Wang, K.K.W., Diaz-Arrastia, R., Okonkwo, D.O., Jain, S., and Manley, G.T.; TRACK-TBI Investigators. (2019). Association between plasma GFAP concentrations and MRI abnormalities in patients with CT-negative traumatic brain injury in the TRACK-TBI cohort: a prospective multicentre study. Lancet Neurol. 18, 953–961.
21. Yuh, E.L., Mukherjee, P., Lingsma, H.F., Yue, J.K., Ferguson, A.R., Gordon, W.A., Valadka, A.B., Schnyer, D.M., Okonkwo, D.O., Maas, A.I., and Manley, G.T.; TRACK-TBI Investigators. (2013). Magnetic resonance imaging improves 3-month outcome prediction in mild traumatic brain injury. Ann. Neurol. 73, 224–235.
22. Haacke, E.M., Duhaime, A.C., Gean, A.D., Riedy, G., Wintermark, M., Mukherjee, P., Brody, D.L., DeGraba, T., Duncan, T.D., Elovic, E., Hurley, R., Latour, L., Smirniotopoulos, J.G., and Smith, D.H. (2010). Common data elements in radiologic imaging of traumatic brain injury. J. Magn. Reson. Imaging 32, 516–543.
23. Shapiro, E.M., Skrtic, S., Sharer, K., Hill, J.M., Dunbar, C.E., and Koretsky, A.P. (2004). MRI detection of single particles for cellular imaging. Proc. Natl. Acad. Sci. U. S. A. 101, 10901–10906.

24. Edlow, B.L., Mareyam, A., Horn, A., Polimeni, J.R., Witzel, T., Tisdall, M.D., Augustinack, J.C., Stockmann, J.P., Diamond, B.R., Stevens, A., Tirrell, L.S., Folkerth, R.D., Wald, L.L., Fischl, B., and van der Kouwe, A. (2019). 7 Tesla MRI of the ex vivo human brain at 100 micron resolution. Sci. Data 6, 244.
25. Fischl, B., Salat, D.H., van der Kouwe, A.J., Makris, N., Segonne, F., Quinn, B.T., and Dale, A.M. (2004). Sequence-independent segmentation of magnetic resonance images. Neuroimage 23, Suppl. 1, S69–S84.
26. McNab, J.A., Jbabdi, S., Deoni, S.C., Douaud, G., Behrens, T.E., and Miller, K.L. (2009). High resolution diffusion-weighted imaging in fixed human brain using diffusion-weighted steady state free precession. Neuroimage 46, 775–785.
27. McNab, J.A., and Miller, K.L. (2008). Sensitivity of diffusion weighted steady state free precession to anisotropic diffusion. Magn. Reson. Med. 60, 405–413.
28. Deoni, S.C., Peters, T.M., and Rutt, B.K. (2005). High-resolution T1 and T2 mapping of the brain in a clinically acceptable time with DESPOT1 and DESPOT2. Magn. Reson. Med. 53, 237–241.
29. McNab, J.A., Edlow, B.L., Witzel, T., Huang, S.Y., Bhat, H., Heberlein, K., Feiweier, T., Liu, K., Keil, B., Cohen-Adad, J., Tisdall, M.D., Folkerth, R.D., Kinney, H.C., and Wald, L.L. (2013). The Human Connectome Project and beyond: initial applications of 300mT/m gradients. Neuroimage 80, 234–245.
30. Dale, J.M., and Garcia, M.L. (2012). Neurofilament phosphorylation during development and disease: which came first, the phosphorylation or the accumulation? J. Amino Acids 2012, 382107.
31. McNab, J.A., Polimeni, J.R., Wang, R., Augustinack, J.C., Fujimoto, K., Stevens, A., Triantafyllou, C., Janssens, T., Farivar, R., Folkerth, R.D., Vanduffel, W., and Wald, L.L. (2013). Surface based analysis of diffusion orientation for identifying architectonic domains in the in vivo human cortex. Neuroimage 69, 87–100.
32. Schindelin, J., Arganda-Carreras, I., Frise, E., Kaynig, V., Longair, M., Pietzsch, T., Preibisch, S., Rueden, C., Saalfeld, S., Schmid, B., Tinevez, J.Y., White, D.J., Hartenstein, V., Eliceiri, K., Tomancak, P., and Cardona, A. (2012). Fiji: an open-source platform for biological-image analysis. Nat. Methods 9, 676–682.
33. Johnson, V.E., Stewart, W., Weber, M.T., Cullen, D.K., Siman, R., and Smith, D.H. (2016). SNTF immunostaining reveals previously undetected axonal pathology in traumatic brain injury. Acta Neuropathol. 131, 115–135.
34. Greer, J.E., McGinn, M.J., and Povlishock, J.T. (2011). Diffuse traumatic axonal injury in the mouse induces atrophy, c-Jun activation, and axonal outgrowth in the axotomized neuronal population. J. Neurosci. 31, 5089–5105.
35. Mac Donald, C.L., Dikranian, K., Song, S.K., Bayly, P.V., Holtzman, D.M., and Brody, D.L. (2007). Detection of traumatic axonal injury with diffusion tensor imaging in a mouse model of traumatic brain injury. Exp. Neurol. 205, 116–131.
36. Zhang, J., Jones, M., DeBoy, C.A., Reich, D.S., Farrell, J.A., Hoffman, P.N., Griffin, J.W., Sheikh, K.A., Miller, M.I., Mori, S., and Calabresi, P.A. (2009). Diffusion tensor magnetic resonance imaging of Wallerian degeneration in rat spinal cord after dorsal root axotomy. J. Neurosci. 29, 3160–3171.
37. Haber, M., Hutchinson, E.B., Sadeghi, N., Cheng, W.H., Namjoshi, D., Cripton, P., Irfanoglu, M.O., Wellington, C., Diaz-Arrastia, R., and Pierpaoli, C. (2017). Defining an analytic framework to evaluate quantitative MRI markers of traumatic axonal injury: preliminary results in a mouse closed head injury model. eNeuro 4, ENEURO .0164-17.2017.
38. Bennett, R.E., Mac Donald, C.L., and Brody, D.L. (2012). Diffusion tensor imaging detects axonal injury in a mouse model of repetitive closed-skull traumatic brain injury. Neurosci. Lett. 513, 160–165.
39. Holleran, L., Kim, J.H., Gangolli, M., Stein, T., Alvarez, V., McKee, A., and Brody, D.L. (2017). Axonal disruption in white matter underlying cortical sulcus tau pathology in chronic traumatic encephalopathy. Acta Neuropathol. 133, 367–380.
40. Shin, S.S., Verstynen, T., Pathak, S., Jarbo, K., Hricik, A.J., Maserati, M., Beers, S.R., Puccio, A.M., Boada, F.E., Okonkwo, D.O., and Schneider, W. (2012). High-definition fiber tracking for assessment of neurological deficit in a case of traumatic brain injury: finding, visualizing, and interpreting small sites of damage. J. Neurosurg. 116, 1062–1069.
41. Marmarou, C.R., Walker, S.A., Davis, C.L., and Povlishock, J.T. (2005). Quantitative analysis of the relationship between intra- axonal neurofilament compaction and impaired axonal transport following diffuse traumatic brain injury. J. Neurotrauma 22, 1066–1080.
42. Ziogas, N.K., and Koliatsos, V.E. (2018). Primary traumatic axonopathy in mice subjected to impact acceleration: a reappraisal of pathology and mechanisms with high-resolution anatomical methods. J. Neurosci. 38, 4031–4047.
43. Weber, M.T., Arena, J.D., Xiao, R., Wolf, J.A., and Johnson, V.E. (2019). CLARITY reveals a more protracted temporal course of axon swelling and disconnection than previously described following traumatic brain injury. Brain Pathol. 29, 437–450.
44. Griffin, A.D., Turtzo, L.C., Parikh, G.Y., Tolpygo, A., Lodato, Z., Moses, A.D., Nair, G., Perl, D.P., Edwards, N.A., Dardzinski, B.J., Armstrong, R.C., Ray-Chaudhury, A., Mitra, P.P., and Latour, L.L. (2019). Traumatic microbleeds suggest vascular injury and predict disability in traumatic brain injury. Brain 142, 3550–3564.
45. Johnson, V.E., Weber, M.T., Xiao, R., Cullen, D.K., Meaney, D.F., Stewart, W., and Smith, D.H. (2018). Mechanical disruption of the blood-brain barrier following experimental concussion. Acta Neuropathol. 135, 711–726.
46. Boyko, O.B., Alston, S.R., Fuller, G.N., Hulette, C.M., Johnson, G.A., and Burger, P.C. (1994). Utility of postmortem magnetic resonance imaging in clinical neuropathology. Arch. Pathol. Lab. Med. 118, 219–225.
47. Dawe, R.J., Yu, L., Leurgans, S.E., Schneider, J.A., Buchman, A.S., Arfanakis, K., Bennett, D.A., and Boyle, P.A. (2016). Postmortem MRI: a novel window into the neurobiology of late life cognitive decline. Neurobiol. Aging 45, 169–177.
48. Gangolli, M., Holleran, L., Hee Kim, J., Stein, T.D., Alvarez, V., McKee, A.C., and Brody, D.L. (2017). Quantitative validation of a nonlinear histology-MRI coregistration method using generalized Q-sampling imaging in complex human cortical white matter. Neuroimage 153, 152–167.

Address correspondence to:
Amber L. Nolan, MD, PhD
Harborview Medical Center Neuropathology
Box 359791
325 Ninth Avenue
Seattle, WA 98104
USA

E-mail: nolanam@uw.edu